

What will the next generation radio telescope detect at 1.4 GHz?

A. Hopkins (ahopkins@atnf.csiro.au)

Australia Telescope National Facility, PO Box 76 Epping, NSW 1710, Australia.

R. Windhorst

Dept. of Physics and Astronomy, Arizona State University, Box 871504, Tempe, AZ 85287-1504, USA

L. Cram

Astrophysics Department, School of Physics, University of Sydney, NSW 2006, Australia

R. Ekers

Australia Telescope National Facility, PO Box 76 Epping, NSW 1710, Australia.

Abstract. An international project is underway to design and build a radio telescope with an effective collecting area two orders of magnitude greater than the largest existing instruments. One of the many scientific goals of this instrument will be the investigation of the extragalactic radio source population at flux densities two to three orders of magnitude fainter than the limits of existing observations. We present simulations of the radio sky at 1.4 GHz down to a flux density limit of $0.1 \mu\text{Jy}$ using extrapolations of known radio luminosity functions for two different population scenarios. The resulting simulations confirm that a resolution of $0.^{\prime\prime}1$ is necessary to avoid formal confusion, but source blending may still dominate if the intrinsic size of such faint sources is larger than a few kiloparsecs.

Keywords: galaxies: evolution — galaxies: general — galaxies: luminosity function

1. Introduction

New developments in all fields of astronomy have brought the current generation of astronomers to the brink of probing the origin and evolution of the Universe as a whole. Many new instruments, both ground- and space-based, are being designed and built to facilitate these studies, and it has long been recognised that major scientific advances follow such technical innovation (Harwit, 1981; de Solla Price, 1963, for example). To maintain the extraordinary momentum of discovery of the last few decades in the metre and centimetre wavelength regime, a very large new radio telescope will be needed, having a sensitivity 100 times better than existing premier radio telescopes. An increase in sensitivity of this order cannot be achieved by improving the electronics of receiver systems, but only by having a radio telescope with



© 2021 Kluwer Academic Publishers. Printed in the Netherlands.

a total effective collecting area of about a million square metres. The instrument has therefore acquired the appellation the “Square Kilometre Array” (SKA). The time by which such a new international world radio observatory is needed to complement other planned instruments will be in the years around 2010. The international effort to design and build the SKA has been growing and progressing since 1993, when the International Union for Radio Science (URSI) established the Large Telescope Working Group to begin developing scientific goals and technical specifications for the next generation radio observatory.

A more detailed introduction to the SKA project, including preliminary specifications, is given by Braun and Taylor (1999), who outline the SKA concept and present a wide range of the scientific questions such an instrument could address. These include a number of key goals, such as establishing the redshift of reionisation (Shaver et al., 1999, for example), detection of the precursors of the first galaxies through HI, measuring the mass function of black holes in galaxy cores, pulsar detection and timing in other galaxies as well as our own, and investigation of star-formation processes and radio emission from stars, among many others no less inspiring (Braun and Taylor, 1999; Hopkins et al., 1999c). In addition, there will be unanticipated discoveries that may represent the most significant results from the instrument. Since we cannot predict the nature of serendipitous discoveries, however, we are limited to investigating identified goals. This paper investigates the implications of our current knowledge about extragalactic radio source populations on the results of anticipated 1.4 GHz radio continuum observations with such an instrument. This frequency has been chosen since it is one of the most well studied, with radio source counts measured over almost seven orders of magnitude.

A number of published radio surveys probe the population of micro-jansky (< 0.1 mJy) radio sources (Windhorst et al., 1993a; Windhorst et al., 1995; Richards et al., 1998; Hopkins et al., 1998; Hopkins et al., 1999b; Norris et al., 1999). Below a few mJy, the 1.4 GHz population begins to be dominated by starburst and disk galaxies, whose radio emission derives primarily from star formation processes (Windhorst et al., 1985; Kron et al., 1985; Benn et al., 1993; Fomalont et al., 1997; Georgakakis et al., 1999), as opposed to the classical radio sources fuelled by active galactic nuclei (AGN), which dominate at higher flux densities. Interest in the sub-millijansky population stems from the desire to investigate the nature and history of star-formation in galaxies, and the potential exists through radio-selection to provide very large, homogeneously selected samples of actively star-forming galaxies over a wide range in redshift. While current surveys are only just starting to compile large samples, approaching thousands of objects (Georgakakis

et al., 1999; Hopkins et al., 1999b), the anticipated sensitivity at nJy levels, resolution of $0''.1$, and field size of one square degree at 1.4 GHz, imply that surveys with the SKA will rapidly dwarf present surveys. To investigate the issues surrounding source confusion and dynamic range limitations in such surveys, we use extrapolations of current models describing the 1.4 GHz radio population, and have begun a program of simulating aspects of the radio sky at this wavelength. Throughout this paper we use $H_0 = 50 \text{ km s}^{-1} \text{ Mpc}^{-1}$ and $q_0 = 0.5$.

2. The model

The local 1.4 GHz luminosity function (LF) is well determined down to $L \approx 10^{18.5} \text{ W Hz}^{-1}$ (Condon, 1989). LFs invoking luminosity evolution models for the AGN population (Dunlop and Peacock, 1990) and the starburst population (Rowan-Robinson et al., 1993; Hopkins et al., 1998) match the observed 1.4 GHz source counts down to the flux density limits of current observation, and we have adopted these models for our investigation. We have extrapolated these 1.4 GHz LFs to luminosities much fainter than have been observed, and supplemented them with distributions in linear size of the objects. This effectively provides a “model universe,” which is then projected onto the desired two-dimensional field of view. Although the effects of large-scale structure have been ignored in this initial model, they will be included as the work is refined, adding the ability to test various clustering models against observation. The model also allows the simulation of different cosmologies, and different rates and types of evolution for direct comparison to observation. In practice, though, this requires the development of different luminosity function models and evolutionary rates for each cosmology of interest, to ensure the source counts predicted from the model are consistent with existing observations.

2.1. RADIO SOURCE POPULATIONS

The galaxy populations used for our simulations comprise four distinct types of radio sources that we broadly classify as “AGN” or “starforming” according to whether the radio emission for the population is derived predominantly from a central engine or from star-formation processes, respectively. We have divided the AGN class into steep-spectrum and flat-spectrum radio sources, following Dunlop and Peacock (1990). The LFs corresponding to these two populations have

the form (Dunlop and Peacock, 1990):

$$\phi = \phi_0 \left\{ \left(\frac{L_{1.4}}{L_c(z)} \right)^\alpha + \left(\frac{L_{1.4}}{L_c(z)} \right)^\beta \right\}^{-1}, \quad (1)$$

with parameters

$$\begin{aligned} \phi_0 &= 10^{-6.91}, \\ \alpha &= 0.69, \\ \beta &= 2.17, \\ L_c(z) &= 26.22 + 1.26z - 0.26z^2, \end{aligned}$$

for steep spectrum AGN, and

$$\begin{aligned} \phi_0 &= 10^{-8.15}, \\ \alpha &= 0.83, \\ \beta &= 1.96, \\ L_c(z) &= 26.36 + 1.18z - 0.28z^2, \end{aligned}$$

for flat spectrum AGN. The luminosity evolution of this population is included in the redshift dependence of $L_c(z)$. This evolution results in a redshift cutoff in the population beyond $z \approx 2$ (Dunlop and Peacock, 1990), which can be seen in the redshift distributions from the simulations (Section 3).

The starforming class includes what we refer to as “IRAS-type” galaxies, for which we have used the $60\mu\text{m}$ “warm IRAS” galaxy luminosity function of Saunders et al. (1990), after conversion to 1.4 GHz assuming $L_{60} = 100L_{1.4}$ (Rowan-Robinson et al., 1993). This IRAS-type population is identified with the “starburst” galaxy population that begins to dominate the 1.4 GHz source counts below a few millijanskies. Their luminosity function has the form (Saunders et al., 1990; Rowan-Robinson et al., 1993):

$$\phi(L) = C \left(\frac{L}{L^*} \right)^{1-\alpha} \exp \left[-\frac{1}{2\sigma^2} \log_{10}^2 \left(1 + \frac{L}{L^*} \right) \right], \quad (2)$$

with parameters (assumed the same at $60\mu\text{m}$ and 1.4 GHz) of $\alpha = 1.27$, $\sigma = 0.626$, and $C = 3.25 \times 10^{-2}$. At $60\mu\text{m}$, $L_{60}^* = 10^{23.9} \text{ W Hz}^{-1}$ so from the radio/FIR correlation, $L_{1.4}^* = 10^{21.9} \text{ W Hz}^{-1}$. The luminosity evolution for this population is of the form $L(z) \propto (1+z)^Q$ with $Q = 3.3$. A form of redshift cutoff at $z = 2$ was used in this evolution, also. For $z > 2$ the evolution was calculated as though the source was at $z = 2$, i.e. $L(z \geq 2) \propto (1+2)^Q$ (Hopkins et al., 1998).

Radio emission produced through star-formation processes can be interpreted as an indicator of the current star-formation rate (SFR) in a galaxy if no AGN emission is present (Cram et al., 1998). Hence, as observational sensitivity improves, the so-called “normal” galaxies will eventually be detectable through their radio emission even though their SFRs may be quite low. The population of normal galaxies so detected may be adequately represented by the faint end tail of the “warm IRAS” luminosity function, and we have constructed several simulations under this assumption. There is the alternative possibility that an additional luminosity function needs to be invoked to account for galaxies with only modest levels of star formation. Certainly the radio source counts derived only from the “warm IRAS” luminosity function (combined with the AGN population) lie well below the upper limit derived from limits on the cosmic background radiation (CBR) fluctuations (Fomalont et al., 1993; Windhorst et al., 1993b; Windhorst, 1999).

To include these modest starformers in our simulations, we have chosen to use the known luminosity function for optical galaxies, the great majority of which have low SFRs. Accurately modelling the radio properties from the optical LF, however, requires a knowledge of the bivariate (radio-optical) luminosity function (BLF) over a large range of luminosities. Despite the limits to the current knowledge of the BLF (Auriemma et al., 1977; Sadler et al., 1989; Hopkins et al., 1999b), an attempt to include this population was made using an over-simplified model: the assumption of a constant radio/optical luminosity ratio. One possibility for refining this assumption could be to use a luminosity ratio distribution closer to the observed distribution in the far-infrared/optical luminosity ratio (Corbelli et al., 1991; Rowan-Robinson et al., 1987), by invoking the radio/FIR correlation, although we have not explored this extra parameter space in the current investigation. The optical (B_J -band) luminosity function used (Efstathiou et al., 1988) was a Schechter function with parameters $\alpha = -1.1$, $\phi^* = 0.0156$ and $M^* = -19.9$ mag, which corresponds to $L^* = 10^{21.5} \text{ W Hz}^{-1}$ at 440 nm. The luminosity ratio chosen was $L_{1.4}/L_{opt} = \frac{1}{3}$ (for $L_{1.4}$ and L_{opt} in units of W Hz^{-1}), which corresponds to a SFR of $\approx 0.26 M_{\odot} \text{ yr}^{-1}$ for an optical L^* galaxy (from equation 1 of Cram et al., 1998). This ratio is the highest possible (constant) value consistent with the observed counts and the contributions from the other populations. The resulting luminosity function (with no evolution invoked), combined with the other populations, has been used to predict the source counts to a flux density of 1 nJy (Figure 1). The symbols in this Figure come from two main sources, the crosses are a compilation of 1.4 GHz source counts from Windhorst et al. (1993a), and the circles from the *Phoenix*

Deep Survey (Hopkins et al., 1999b, and references therein). The thick dashed line shown in this and succeeding Figures is the upper limit to the source counts derived from known limits to the CBR fluctuations (Fomalont et al., 1993; Windhorst et al., 1993b; Windhorst, 1999). If the source count continues toward fainter flux densities from the limits of existing observations with the constant slope seen between about 0.05–1 mJy ($\gamma = 2.3$, where the differential source counts $n(S) \propto S^{-\gamma}$), then the count must ultimately converge below about 100 nJy (± 0.5 dex) with a slope $\gamma \leq 2$.

It is possible that there could be a greater contribution from the normal galaxy population if the rate of luminosity evolution invoked for the IRAS-type galaxies were lower. Such a scenario is reflected in the source counts shown in Figure 2. Here we show source counts predicted under the assumption that the IRAS-type galaxies undergo luminosity evolution at a rate $L(z) \propto (1+z)^Q$ with $Q = 2.9$ rather than the $Q = 3.3$ rate used in Figure 1. The luminosity ratio used for the normal galaxies in Figure 2 is $L_{1.4}/L_{opt} = 0.8$ (corresponding to a SFR of $\approx 0.63 M_{\odot}\text{yr}^{-1}$ for an optical L^* galaxy). Uncertainty in the $60\text{ }\mu\text{m}$ luminosity function normalisation leads to an uncertainty in the magnitude of the predicted source counts. This is indicated by the vertical error bar shown on the counts for the IRAS-type galaxies. Any additional population should not increase the contribution of the starforming galaxies outside this range.

The faintest counts due to the starforming populations could alternatively be *even lower* than predicted here if supernovae in low-mass galaxies are efficient at removing gas (Babul and Rees, 1992, but see also Mac Low and Ferrara, 1998). In any case it is worth remembering that there are still many parameters that are not yet observationally constrained, and we have restricted this investigation to predictions from only two scenarios. These scenarios both include the two components of the AGN population, combined with a starforming population being composed of (1) IRAS-type galaxies only, and (2) IRAS-type galaxies plus normal galaxies with $L_{1.4}/L_{opt} = \frac{1}{3}$.

2.2. LINEAR SOURCE SIZES

The distribution in linear size of radio sources at 1.4 GHz has been studied extensively for the population we are referring to as AGN. Indeed, the variation in angular size of radio sources with redshift is a classic test for investigating cosmological models (Hooley et al., 1978, for example). In more recent work describing the variation of linear size with redshift (Gopal-Krishna, 1991; Kapahi, 1989; Onuora, 1989; Singal, 1988; Oort et al., 1987; Allington-Smith, 1984, for example)

the general consensus is that for $z \lesssim 1.5$ the linear size of these (steep-spectrum) radio sources evolves as

$$l = \frac{l_0}{(1+z)^3} P^{0.3}, \quad (3)$$

(see also Subramanian and Swarup, 1990). Here l is the proper length of the galaxy. This relation reflects the evolution of the characteristic length (l_0) of the steep-spectrum AGN population, combined with the distribution (dependent on P) of individual source sizes within that population. A value of $l_0 = 3 \times 10^{-6} \text{ kpc} (\text{W Hz}^{-1})^{-0.3}$ was used for consistency with Subramanian and Swarup (1990). In our simulations we have adopted this relationship for $z < 1.5$. For larger redshifts, $z = 1.5$ was used when calculating the intrinsic linear size of a source (i.e. $l = l_0 / (1+1.5)^3 P^{0.3}$). The angular size for each source is derived from its intrinsic linear size, l , in Mpc, and its actual redshift, z , by

$$\theta = l \frac{(1+z)^2}{d_L}, \quad (4)$$

where d_L is the luminosity distance

$$d_L = \frac{c}{H_0 q_0^2} (q_0 z + (q_0 - 1)(\sqrt{1 + 2q_0 z} - 1)). \quad (5)$$

Some recent work (Blundell et al., 1999) suggests that the above parametrisation of linear size is too simplistic and is biased by catalogue specific selection effects, although these conclusions are more applicable at frequencies lower than 1.4 GHz. For this reason we neglect the results of Blundell et al. (1999) in our present simulations, and this should be kept in mind when they are presented in Section 3.

There is evidence that, in galaxies with higher levels of star-formation activity, this activity is concentrated in smaller regions than for less active galaxies (van Driel et al., 1991). For the more modest starforming galaxies the extent of the radio emission (coming predominantly from supernovae and HII regions) is likely to be larger, but primarily restricted to the size of the optical disk. For the IRAS-type population a distribution of 1.4 GHz linear sizes was derived from the radio sizes of IRAS galaxies (van Driel et al., 1991; Eales et al., 1988), and a distribution of half-light radii for disk galaxies (Roche et al., 1998) was used for the normal galaxy population. These distributions are both luminosity dependent, and are quite different to those used above for the steep-spectrum AGN. The relation for IRAS-types was drawn from Figure 4 of van Driel et al. (1991) and converted to 1.4 GHz using a spectral index of -0.7 giving:

$$\log(l) = 0.5 \log(L_{1.4}) - 10.8 \quad (6)$$

where l is the linear size in kpc and $L_{1.4}$ the luminosity in WHz^{-1} . This relation was also used for the flat-spectrum AGN population, which is typically composed of quite compact sources. The relation for the normal galaxies is

$$\log(r_{\text{hl}_0}) = -0.2M_B - 3.30 \quad (7)$$

and using an evolution of the half-light radius, r_{hl_0} , of the form $r_{\text{hl}} = (1 - 0.2z)r_{\text{hl}_0}$ approximated from Figure 2 of Roche et al. (1998). This evolution was truncated at $z = 4$ so that beyond this limit r_{hl} was calculated as though the source was at $z = 4$. These parametrisations are intended to be representative rather than exhaustive, as obviously galaxies of the same luminosity can have quite different physical sizes. The values determined for the IRAS-type galaxies are typically an order of magnitude smaller than those for the normal population, consistent with the result found by Eales et al. (1988) that radio sizes of high FIR luminosity IRAS sources are about a tenth the size of the optical galaxy. This is also consistent with the result that in disk galaxies the scale-length of the disk is about ten times the effective radius of the bulge (de Jong, 1996, Figure 18, particularly K-band results, which are less likely to be affected by extinction).

The resulting simulations are quite sensitive to the distributions chosen here, as the numbers of starforming galaxies are very large when faint flux density limits are chosen. Accordingly, this aspect of the simulation would benefit from a more accurate parametrisation of the linear sizes of faint optical galaxies as a function of luminosity and redshift.

2.3. SIMULATED IMAGES

To construct simulated images, the luminosity functions and evolutionary models are used to define the number, luminosity and redshift of sources in a specified field of view, above a given flux density limit. The luminosities are combined with redshifts and the chosen cosmology to produce flux densities for each source. Similarly, the intrinsic sizes are used to derive apparent angular sizes for each source. Each source is represented in the image by a two-dimensional gaussian distribution of the total flux density, with random position angle. The apparent ellipticity distribution of faint field galaxies changes very little from $B = 15$ to $B = 27$ mag (Odewahn et al., 1997), so in a sense the distribution of ellipticities is intrinsically random and hardly affected by evolutionary effects, even though the galaxy morphology changes noticeably between $B = 15$ and $B = 27$. To model the observed axial ratio, R , of the gaussian for disk systems we refer to the results of

Lambas et al. (1992) who find that a pure oblate model for disk galaxies fails to reproduce the observed axial ratios. However, a nearly oblate model with intrinsic axial ratio $r = 0.2$ can produce consistent fits to the observations. Binney and de Vaucouleurs (1976) also find a range $0.15 < r < 0.35$ derived for spiral galaxies from the Second Reference Catalogue of Bright Galaxies (de Vaucouleurs et al., 1976), and state that later type spirals have distributions that peak at smaller values of r . For simplicity, then, we have assumed each disk is an oblate ellipsoid with intrinsic axial ratio of $r = 0.2$. A random angle of inclination, i , is chosen which then gives the observed axial ratio, R , as

$$R = \sqrt{r^2 + (1 - r^2) \cos^2 i}. \quad (8)$$

The source so constructed is randomly positioned within the specified field of view, and coloured according to type, red for AGNs and blue for starformers. If sources overlap, their flux densities are simply added together, producing appropriate colour combinations if they are not the same colour source. No attempt to include the effects of obscuration or gravitational lensing has been made, although these could in principle be added to the model.

In addition, as an elementary step toward modelling the double-lobed nature of many real AGNs, a pair of adjacent elliptical gaussians have been used for the steep spectrum sources, rather than the single elliptical gaussian used for flat spectrum AGNs and starformers. This is an unrealistic over-simplification, particularly as no orientation effects, beaming, or more complicated morphologies have been contemplated. The usefulness of refinements to this aspect of the display can be debated, but for the current purpose this simple step was deemed sufficient.

3. Simulations

The algorithm described above has been used to create simulated radio images for a wide variety of field sizes and flux density limits. Many simulations were investigated but here we present only two, indicative of our results, for analysis in terms of the properties of the SKA.

The first example is shown in Figure 3, a simulation with a field size of $5' \times 5'$, about four times the size of the Hubble Deep Field (HDF) (c.f. Richards et al., 1998). For this simulation the starformers are represented by the IRAS-type population only. A flux density limit of $0.1 \mu\text{Jy}$ has been used and over 1000 sources brighter than this limit are predicted (a source density of $\sim 4.8 \times 10^8 \text{ sr}^{-1}$). Consistency checks have been performed to confirm that the simulated distributions in flux

density agree with the models used to produce them. Source counts for the simulation in Figure 3 are shown in Figure 4 along with the (continuous) source counts derived from the assumed luminosity functions and evolution. Typical luminosity and redshift distributions have been derived from the simulations and are presented in Figure 5.

A second simulation of a $5' \times 5'$ region is shown in Figure 6, again with a flux density limit of $0.1 \mu\text{Jy}$, this time including the population of normal galaxies. A total of 1941 sources (574 AGNs, 1367 starformers) are predicted, giving a source density of $\sim 9.2 \times 10^8 \text{ sr}^{-1}$. Again, source counts, luminosity and redshift distributions are shown (Figures 7 and 8). It can be seen that even with this scenario and at these faint levels, while the starformer population is dominant the AGN population is certainly not negligible. A hint of this effect may be seen in recent work in the optical domain (Sarajedini et al., 1999) showing that $\approx 10\%$ of HST Medium Deep Survey galaxies (to $z \approx 0.8$) may be low luminosity AGNs (implied through the presence of unresolved nuclear components that contribute noticeably to the total galaxy light). There is also a very clear distinction between the two scenarios (starformers comprising IRAS-types only compared to the inclusion of a normal galaxy population) in terms of the number of sources predicted. This is a prediction that will easily distinguish between the scenarios when SKA observations are eventually made.

The absence of very large and bright AGN-type sources in the simulated fields shown is a result of presenting simulated fields coincidentally free of such objects. This mimics the careful selection against bright sources typical in deep radio surveys, as well as ensuring clarity in the displayed simulations. Typically a simulated field of this size may contain one or two sources of several tens of millijanskies, and with physical sizes dominating the field.

The limiting flux density value of $0.1 \mu\text{Jy}$ was chosen for a variety of reasons. Primarily, the consistency of our simulations with existing observations (to levels of $50 \mu\text{Jy}$) implies a reasonable reliability to levels of about $1 \mu\text{Jy}$, so a level at least an order of magnitude fainter is necessary to extend the simulations into a new regime, where the dominant population is truly unknown, and where the actual properties of the high-redshift universe may be revealed by future observations. Also, for an interferometer having the specifications given for the SKA, $0.1 \mu\text{Jy}$ is the expected 5σ level achievable after a 12 hour integration. The relevant specifications are an effective area to system temperature ratio of $A_{\text{eff}}/T_{\text{sys}} = 2 \times 10^4 \text{ m}^2\text{K}^{-1}$ with two simultaneous frequency bands and a bandwidth $\Delta\nu = 500 \text{ MHz}$ at 1.4 GHz (Braun and Taylor, 1999). Images deeper than this $0.1 \mu\text{Jy}$ level will obviously be attainable through longer integrations with the instrument, (although predictions

to such levels are likely to suffer from increasing uncertainties in the extrapolations). For example, the time spent observing the HDF with the Very Large Array (Richards et al., 1998) was 152 hours. Some recent observations of similar integration time with the Australia Telescope Compact Array are provided by Hopkins et al. (1999b) and Norris et al. (1999). With the potential to reach a 5σ detection level of about 30 nJy over such an integration time, dynamic range considerations for the SKA will be very important! In the HDF observations, the VLA was dynamic range limited at a level of 10,000:1. The ATCA deep field observations of the HDF-S are not yet dynamic range limited, but have a thermal noise limit of 10,000:1. A dynamic range of 100,000:1 has been reached by ATCA in other wide field images. Although no insurmountable technical difficulties are anticipated in reaching the required levels of 10⁶:1 or 10⁷:1 on axis, achieving similar values at the half-power level will be more difficult, and this is an aspect of the project which deserves close attention (see also de Bruyn, 1996).

4. Discussion

In each simulation shown, the brightest source is an AGN, but between luminosities of about 10^{22} WHz⁻¹ and $10^{24.5}$ WHz⁻¹ the IRAS-types dominate (see Figures 5 and 8). This result can be explained as a combination of the small area being sampled (as the bright AGNs have a low surface density), and the dearth of AGN-type galaxies further than $z \approx 3$. This redshift cutoff in the distribution of AGNs results from the chosen model of luminosity evolution for this population (Dunlop and Peacock, 1990). The redshift distribution for the “normal” galaxies (Figure 8) on the other hand, which shows no objects further than redshifts of $z \approx 2$ in these simulations, is not a result of the models used but is instead dependent on the flux density limits chosen for the simulation. Had the limits been fainter, such objects (having only modest intrinsic luminosities, predominantly $< 10^{22}$ WHz⁻¹, as can be seen from the luminosity distribution in Figure 8) would have been detected at continually higher redshifts. Additionally, the distribution of luminosities for this population is very narrow, concentrated primarily within two orders of magnitude. This reflects the shape of the optical luminosity function from which this population is derived, and it is useful to emphasise the very small range of intrinsic luminosities displayed by galaxies at optical wavelengths compared to the range of ten orders of magnitude or more possible in a galaxy’s intrinsic radio luminosity.

Table I. Specifications necessary for a radio telescope able to image a one square degree field of view to a limiting 5σ flux density of S_{\min} in a 12 hr integration.

S_{\min} (μJy)	N	DR	$A_{\text{eff}}/T_{\text{sys}}$ (m^2K^{-1})	θ_{\min} ($''$)	B_{\max} (km)
1.00	360	10^5	2×10^3	1.5	30
0.10	1941	10^6	2×10^4	0.6	70
0.01	9431	10^7	2×10^5	0.3	150

Table I shows how the number of sources increases as the limiting (5σ) flux density is reduced, in the scenario where starformers include both IRAS-types and normal galaxies. Column 3 gives the dynamic range necessary if there will regularly be 100 mJy sources in the (1 square degree) field of view. Very deep radio surveys will obviously continue to be carried out in carefully selected regions, chosen to be free of bright sources. But the specified field of view of 1 square degree at 1.4 GHz implies all but a few areas chosen for deep observations are likely to contain sources of at least several tens of millijanskies. The effective area to system temperature ratio for an instrument which can reach the given limiting flux density in a 12 hour integration is given in column 4 of Table I. Columns 5 and 6 show the minimum resolution and corresponding maximum baseline for operation at 1.4 GHz required to avoid formal (instrumental) confusion, corresponding simply to the number of sources regardless of their apparent sizes. The specification $A_{\text{eff}}/T_{\text{sys}} = 2 \times 10^4 \text{ m}^2\text{K}^{-1}$ corresponds to an effective collecting area of 1 square kilometre with a system temperature of 50 K. This configuration could be used (instead of those in rows 1 and 3 of the Table) to reach the limiting flux densities of 1 μJy and 0.01 μJy by integrating for 7 minutes and 1200 hours, respectively. While a resolution of $0''.6$ is required to avoid formal confusion at the 0.1 μJy level, this would drop to $0''.4$ (and lower for fainter flux density limits) if the source count achieves the maximum level given the CBR limitations. This could arise through new populations not included in the simulations presented here, or different evolutionary forms or rates to those presented in these simulations.

While the limited overlapping of objects in the simulated images implies that the natural confusion level has not yet been reached for the majority of sources, and only the largest and brightest are likely to be affected, a high resolution ($\sim 0''.1$) is desirable to adequately resolve

superimposed sources, facilitating their study. The extent of the natural confusion is directly related to the intrinsic distribution of linear sizes for the starforming population (as opposed to the models used in these simulations). If the true distribution is dominated by objects with small half-light radii (only a few kpc, c.f. Odewahn et al., 1996) the effects of natural confusion, to the $0.1\,\mu\text{Jy}$ level investigated here, will be mild. If the source count reaches its potential limits, though, the problem could be more significant. For high imaging quality at the faintest flux densities (and smallest angular scales) the SKA will require a high sensitivity response over the longer baselines. This implies that a significant fraction of the collecting area needs to be distributed over baselines up to hundreds of kilometres for operation at 1.4 GHz ($0''.1$ resolution requiring baselines of ~ 440 km). There will also be a conflict between designs optimised for operation at high resolution and for good surface brightness sensitivity, so an optimum solution that best addresses the desires of the astronomical community will need to be established. If the instrument is built with a good response at high resolution, then the effects of confusion will be minimal, and very deep radio surveys with the SKA are much more likely to be dynamic range limited than confusion limited.

The large field of view specified for this instrument is 144 times the area of the simulations presented here, hence observations down to $0.1\,\mu\text{Jy}$ will result in $\sim 3 \times 10^5$ sources per field. This has implications for the nature and sophistication of automated source detection and characterisation algorithms that must be developed to analyse such data. Also, since a well sampled image will have several pixels across a synthesised beam FWHM (say $0''.1$), an image of a one square degree field will be $\sim 10^5 \times 10^5$ pixels in size. Although the tens of gigabytes per image required for storage will not be a problem, visual inspection of entire images at full resolution will become difficult in the extreme, and will likely be reserved for objects denoted as interesting by automated classifiers.

5. Conclusions

We have initiated a program of simulating the 1.4 GHz sky to investigate the implications of existing models for luminosity functions, luminosity evolution and linear size distributions on anticipated observations by the SKA. The results are self-consistent and consistent with observed source counts, although below that level it should be remembered that they are based on *extrapolations*. The corresponding level of uncertainty at ever fainter flux densities will increase, and in

fact we might expect to find something quite new and different when actual observations can be made at these sensitivities. Many simulations have been investigated and two of them presented here. The simulations produced with a flux density limit of $0.1 \mu\text{Jy}$ show fields that are dominated by starforming galaxies, although the proportion of AGN galaxies is still significant, even at such faint flux densities. The level of natural confusion in these fields is very strongly related to the choice of models for intrinsic linear size of the starformers, and deserves closer attention. To model different rates of evolution and different cosmologies, additional luminosity function models that correctly reproduce the observed source counts in each of the chosen scenarios are necessary.

The preliminary specifications for the SKA (Braun and Taylor, 1999) have been discussed in the context of the simulations presented here. There would appear to be only minor problems due to natural confusion at the levels of $0.1 \mu\text{Jy}$, and no problems with instrumental confusion, even at much lower flux densities, if a resolution around $0''.1$ to $0''.3$ is chosen. The large field of view and high resolution will necessarily affect the way images are analysed, reducing the level of visual interpretation.

Acknowledgements

We wish to thank the referee for useful suggestions. AMH and LEC acknowledge financial support from the Australian Research Council and the Science Foundation for Physics within the University of Sydney. RAW acknowledges grant AST-9802963 from the National Science Foundation, and NASA grants GO-5985.01-94A and GO-6609.01-95A from STScI under NASA contract NAS5-26555. The Australia Telescope is funded by the Commonwealth of Australia for operation as a National Facility managed by CSIRO.

References

Allington-Smith J. R.: 1984, *Mon. Not. R. Astron. Soc.* **210**, 611.
 Auriemma C., Perola G. C., Ekers R. D., Fanti R., Lari C., Jaffe W. J., Ulrich M. H.: 1977, *Astron. Astrophys.* **57**, 41.
 Babul A. and Rees M. J.: 1992, *Mon. Not. R. Astron. Soc.* **255**, 346.
 Benn C. R., Rowan-Robinson M., McMahon R. G., Broadhurst T. J., Lawrence A.: 1993, *Mon. Not. R. Astron. Soc.* **263**, 98.
 Binney J. and de Vaucouleurs G.: 1981, *Mon. Not. R. Astron. Soc.* **194**, 679.
 Blundell K. M., Rawlings S., Willott C. J., 1999: *Astron. J.* **117**, 677.

R. Braun and R. Taylor (eds.): 1999 *Square Kilometre Array Radio Telescope – The Science Case* URSI Large Telescope Working Group.

Condon J. J.: 1989, *Astrophys. J.* **338**, 13.

Corbelli E., Salpeter E., Dickey J.: 1991, *Astrophys. J.* **370**, 49.

Cram L., Hopkins A., Mobasher B., Rowan-Robinson M.: 1998 *Astrophys. J.* **507**, 155.

de Bruyn A. G.: 1996, in: N. Jackson and R. J. Davis (eds.) *High Sensitivity Radio Astronomy* Cambridge: Cambridge University Press, p. 233.

de Jong R. S.: 1996, *Astron. Astrophys.* **313**, 45.

de Solla Price D. J.: 1963, *Little science, big science* Columbia University Press

de Vaucouleurs G., de Vaucouleurs A., Corwin H. G.: 1976, *Second Reference Catalogue of Bright Galaxies*, University of Texas Press, Austin

Dunlop J. S. and Peacock J. A.: 1990, *Mon. Not. R. Astron. Soc.* **247**, 19.

Eales S. A., Wynn-Williams C. G., Beichman C. A.: 1988, *Astrophys. J.* **328**, 530.

Efstathiou G., Ellis R. S., Peterson B. A.: 1988, *Mon. Not. R. Astron. Soc.* **232**, 431.

Fomalont E. B., Partridge R. B., Lowenthal J. D., Windhorst R. A., Partridge R. B.: 1993, *Astrophys. J.* **404**, 8.

Fomalont E. B., Kellermann K. I., Richards E. A., Windhorst R. A., Partridge R. B.: 1997, *Astrophys. J.* **475**, L5.

Georgakakis A., Mobasher B., Cram L., Hopkins A., Lidman C., Rowan-Robinson M.: 1999, *Mon. Not. R. Astron. Soc.*, (in press)

Gopal-Krishna: 1991, *Astron. Astrophys.* **248**, 415.

Harwit M.: 1981, *Cosmic Discovery. The Search, Scope, and Heritage of Astronomy* (Brighton: Harvester Press)

Hooley A., Longair M. S., Riley J. M.: 1978, *Mon. Not. R. Astron. Soc.* **182**, 127.

Hopkins A. M., Mobasher B., Cram L., Rowan-Robinson M.: 1998, *Mon. Not. R. Astron. Soc.* **296**, 839.

Hopkins A. M., Cram L., Mobasher B., Georgakakis A.: 1999a, in: R. Morganti and W.J. Couch (eds.), *Looking Deep in the Southern Sky* Springer-Verlag, p. 120.

Hopkins A., Afonso J., Cram L., Mobasher B.: 1999b, *Astrophys. J.* **519**, L59.

Hopkins A., Ekers R., Jackson C., Cram L., Green A., Manchester R., Staveley-Smith L., Norris R.: 1999c, *Publ. Astron. Soc. Aus.* (in press)

Kapahi J. A.: 1989, *Astron. J.* **97**, 1.

Kron R. G., Koo D. C., Windhorst R. A.: 1985, *Astron. Astrophys.* **146**, 38.

Lambas D. G., Maddox S. J., Loveday J.: 1992, *Mon. Not. R. Astron. Soc.* **258**, 404.

Mac Low M.-M. and Ferrara A.: 1998, in: D. Breitschwerdt, M. J. Freyberg, J. Truemper (eds.), *The Local Bubble and Beyond* IAU Colloquium 166, Springer-Verlag, p. 559

Norris R., Hopkins A., Sault R., Ekers R., Ekers J., Badia F., Higdon J., Wieringa M., Boyle B., Williams R.: 1999, (in preparation)

Odewahn S. C., Windhorst R. A., Driver S. P., Keel W. C.: 1996, *Astrophys. J.* **472**, L13.

Odewahn S. C., Burstein D., Windhorst R. A.: 1997, *Astron. J.* **114**, 2219.

Onuora L. I.: 1989, *Astrophys. Space Sci.* **162**, 343

Oort M. J. A., Katgert P., Windhorst R. A.: 1987, *Nature* **328**, 500.

Richards E. A., Kellermann K. I., Fomalont E. B., Windhorst R. A., Partridge R. B.: 1998, *Astron. J.* **116**, 1039.

Roche N., Ratnatunga K., Griffiths R. E., Im M., Naim A.: 1998, *Mon. Not. R. Astron. Soc.* **293**, 157.

Rowan-Robinson M., Benn C. R., Lawrence A., McMahon R. G., Broadhurst T. J.: 1993, *Mon. Not. R. Astron. Soc.* **263**, 123.

Rowan-Robinson M., Helou G., Walker D.: 1987, *Mon. Not. R. Astron. Soc.* **227**, 589.

Sadler E. M., Jenkins C. R., Kotanyi C. G.: 1989, *Mon. Not. R. Astron. Soc.* **240**, 591.

Sarajedini V. L., Green R. F., Griffiths R. E., Ratnatunga K.: 1999, *Astrophys. J.* **514**, 746.

Saunders W., Rowan-Robinson M., Lawrence A., Efstathiou G., Kaiser N., Ellis R. S., Frenk C. S.: 1990, *Mon. Not. R. Astron. Soc.* **242**, 318.

Shaver P. A., Windhorst R. A., Madau P., de Bruyn G.: 1999, *Astron. Astrophys.* **345**, 380.

Singal A. K.: 1988, *Mon. Not. R. Astron. Soc.*, **233**, 87.

Subramanian K. and Swarup G.: 1990, *Mon. Not. R. Astron. Soc.* **247**, 237.

van Driel W., van den Broek A. C., de Jong T.: 1991, *Astron. Astrophys. Suppl.* **90**, 55.

Windhorst R. A., Miley G. K., Owen F. N., Kron R. G., Koo D. C.: 1985, *Astrophys. J.* **289**, 494.

Windhorst R. A., Fomalont E. B., Partridge R. B., Lowenthal J. D.: 1993a, *Astrophys. J.* **405**, 498.

Windhorst R. A., Fomalont E. B., Partridge R. B., Lowenthal J. D.: 1993b, in: G. Chincarini, A. Iovino, T. Maccacaro, and D. Maccagni (eds.), *Limits to the 8.4 GHz Nano-Jansky Source Counts and Arcmin-Scale CBR Fluctuations* ASP Conf. Ser. Vol. 51, p. 534.

Windhorst R. A., Fomalont E. B., Kellerman K. I., Partridge R. B., Richards E., Franklin B. E., Pascarelle S. M., Griffiths R. E.: 1995, *Nature* **375**, 471.

Windhorst R. A.: 1999, in: Eds. H. J. A. Röttgering, P. N. Best, M. D. Lehnert (eds.), *The Most Distant Galaxies* Kluwer Academic Publishers, Dordrecht, (in press).

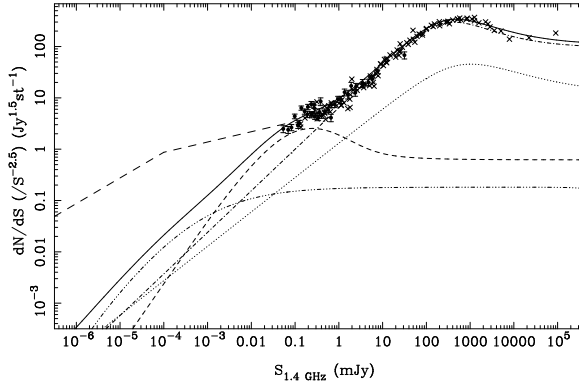


Figure 1. Models of the source counts showing relative contributions of different populations. Thin dashed line: IRAS-type population; Dotted line: AGN flat-spectrum population; Dot-dashed line: AGN steep-spectrum population; Dot-dash-dotted line: normal galaxy population; Solid line: sum of all populations. The symbols are existing observational source counts (see text). The normal galaxy population shown here is the maximum possible contribution supplementary to the other models and consistent with the observations. The thick dashed line represents the upper limit to the source counts implied from CBR constraints. More details are given in the text.

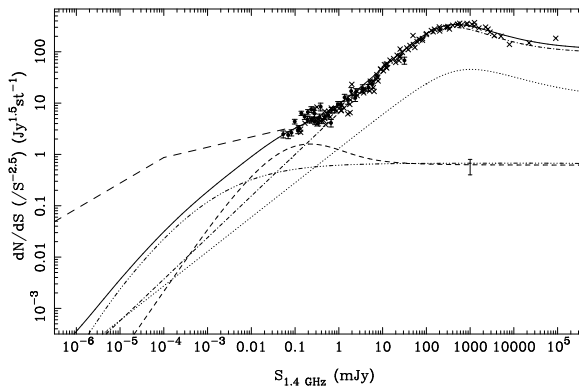


Figure 2. Models of the source counts. Here the evolution of the IRAS-type population is reduced from $Q = 3.3$ to $Q = 2.9$ and a greater contribution is made by the normal galaxies. The error bar shown on the IRAS-type source count indicates the range permitted by the uncertainty in the luminosity function normalisation. See text for details. Symbols and line styles are as for Figure 1. The upper limit to the source counts is again shown as the thick dashed line.

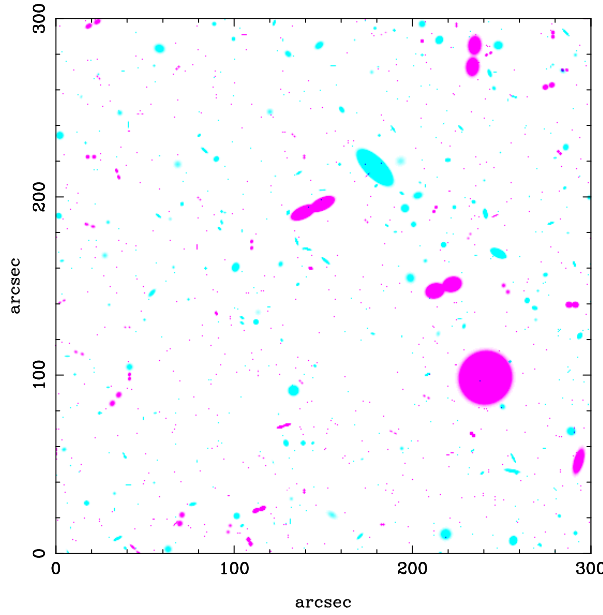


Figure 3. Simulated 1.4 GHz image. The image size is $5'$, with a flux density limit of $0.1 \mu\text{Jy}$. There are 1008 objects in the simulation, divided into two categories: AGN (red, 574 objects) and starformers (blue, 434 objects).

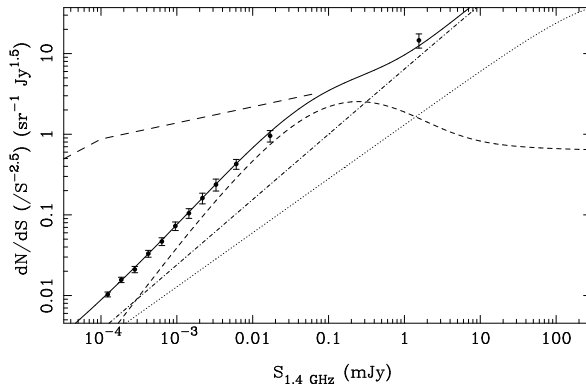


Figure 4. The source counts from the model luminosity functions (line styles as in Figure 1) used to produce the image in Figure 3, along with those calculated from a typical simulation (filled circles showing Poisson error bars), shown to confirm the self-consistency of the simulations. The upper limit to the source counts is again shown as the thick dashed line.

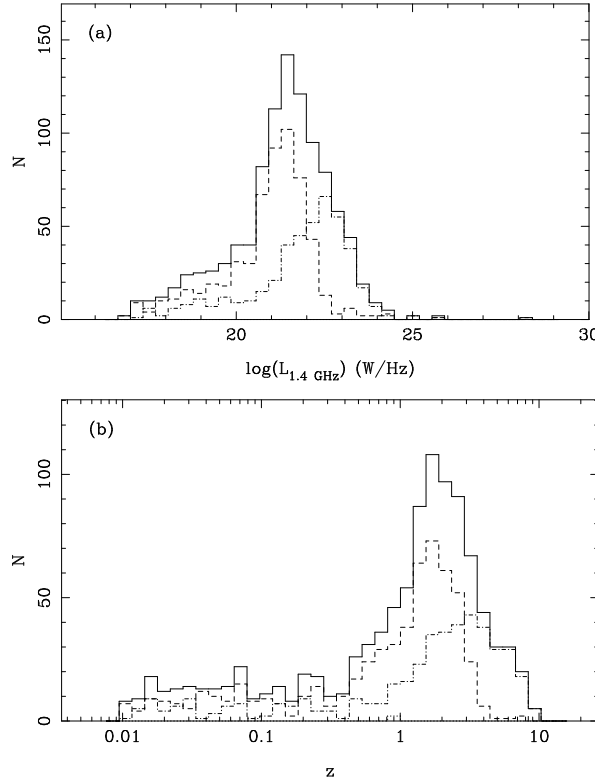


Figure 5. Distribution of (a) luminosities and (b) redshifts for the simulation in Figure 3. The line styles correspond to the different populations. Dashed: AGN; Dot-dashed: IRAS-type; Solid: the sum of all populations.

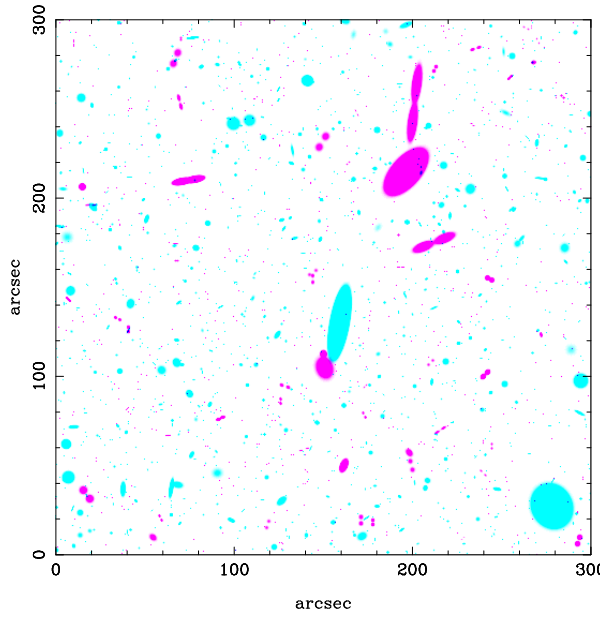


Figure 6. Simulated 1.4 GHz image. This simulation includes the population of normal galaxies in addition to the IRAS-types. The image is 5' on a side, with a flux density limit of $0.1 \mu\text{Jy}$. There are 1941 objects in the simulation, 574 are AGN (red) and 1367 are starformers (blue).

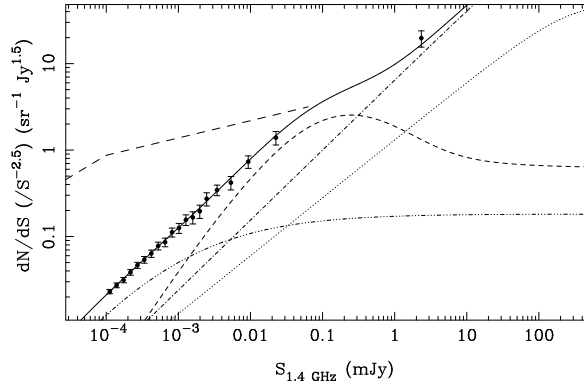


Figure 7. The source counts from the model luminosity functions, along with those calculated from a typical simulation, to confirm the self-consistency of the simulations (c.f. Figure 4). The new population of normal galaxies (dot-dash-dotted line) begins to make a noticeable contribution to the source counts below a few microjanskies. The upper limit to the source counts is again shown as the thick dashed line.

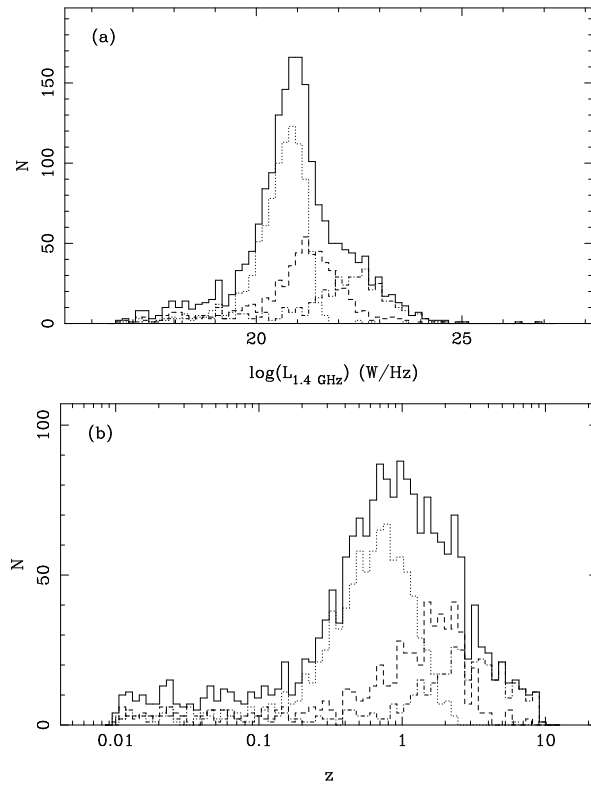


Figure 8. Distributions of (a) luminosity and (b) redshift for simulation in Figure 6. The line styles correspond to the different populations. Dashed: AGN; Dot-dashed: IRAS-type; Dotted: normal galaxies; Solid: the sum of all populations.

